Comparison of LEWICE 1.6 and LEWICE/NS with IRT Experimental Data from Modern Airfoil Tests

William B. Wright
NYMA, Inc.
Brook Park, OH

Mark G. Potapczuk
NASA Lewis Research Center
Cleveland, OH

Abstract

A research project is underway at NASA Lewis to produce a computer code which can accurately predict ice growth under any meteorological conditions for any aircraft surface. The most recent release of this code is LEWICE 1.6. This code is modular in design and can use flow codes other than the default potential flow code. Methods for assessing the capabilities of ice accretion prediction codes are examined by comparing geometric and aerodynamic characteristics of computationally generated and experimentally measured ice shapes. The data used in this paper comes from tests performed in the NASA Lewis Icing Research Tunnel (IRT).

This paper will present comparisons with that data for both ice shape and performance results. A group of geometric characteristics for quantitatively describing ice shape profiles are introduced and used to assess the differences between profiles. An aerodynamic analysis of computational and experimental ice shapes is performed using a structured-grid, Naviér-Stokes, flow code as an alternate method for assessing ice shape similarity. Results indicate that large differences in ice shape are reflected in the resulting aerodynamics but are not necessarily apparent in integrated force parameters such as lift or drag.

Introduction

The Icing Branch at NASA Lewis has undertaken a research project to produce a computer code capable of accurately predicting ice growth under any meteorological conditions for any aircraft surface. The most recent release of this code is LEWICE 1.6 which has now been documented in several reports.[1-3] This paper will not go into the details of the capabilities of this code, as those features are well-described by the previous reports.

The purpose of this paper is to identify and assess criteria which can potentially be used to validate the NASA icing codes. The criteria reviewed in this report are not necessarily the only criteria which can be used for validation but they represent one possible path.

The process for validation of an icing code is quite challenging and is complicated by the fact that no pre-defined acceptance criteria have been identified. To date, evaluation of the performance of ice prediction codes has been based on subjective judgements of the visual appearance of comparisons between ice shapes generated by the code and ice shapes measured in an experimental facility. In order to determine the capabilities of a prediction code it is necessary to develop quantitative measures for the similarity between two ice shapes. The measurement used to make the comparison should be based on the characteristic considered most important for the purposes of the simulation process. For example, design of a thermal ice protection system may dictate that icing limits, accumulation rates, and total collection efficiency are the most important parameters to be simulated while certification of a wing for flight with an ice accretion may require that the ice shape be modeled accurately.

In past reports[1-5], LEWICE has been compared to shapes created in the NASA Lewis Icing Research Tunnel (IRT). While these comparisons have been somewhat favorable, it has not yet been demonstrated that this is all that needs to be done in order to validate LEWICE. Additional comparisons are made in this report, using data from recent tests on an airfoil section representative of a wing section from a business jet, and are examined from a more quantitative approach than has been undertaken in previous efforts. Measured quantities are horn length, horn width, horn angle, stagnation point thickness, and icing limits. This analysis will define the differ-

ences between these shapes and will attempt to associate such differences with the standard qualitative evaluations.

The natural icing environment produces irregular and sometimes chaotic conditions which can not be reproduced in an icing tunnel nor in the current version of LEWICE. However, if the codes can reproduce the same effect on the aircraft as evidenced in flight, then it can be a useful aid for design and potentially for certification purposes. As a result, the performance degradation due to the ice shape is also of interest. It is unclear what magnitude of geometrical difference between computational and experimental ice shapes are significant aerodynamically. Previous studies have shown that glaze and rime accretions can have dramatically different effects on pressure distributions and boundary layer development[6] and hence on lift and drag values.[7] In order to assess these differences, both the LEWICE and IRT shapes examined in the geometric assessment are analyzed with a structured grid, Naviér-Stokes flow code. Comparisons of aerodynamic characteristics of these profiles are then undertaken to identify the important features that should be preserved in a simulation effort.

This paper will attempt to investigate several aspects of this problem. First, a more quantitative comparison is performed between ice shapes generated in the IRT and with LEWICE. Important parameters include horn length, horn width, horn angle, stagnation point thickness, and icing limits. This paper will look at horn size parameters only. This analysis will also define the differences between these shapes which often appear to be qualitatively close to the experimental shapes. Second, both the LEWICE and IRT shapes are analyzed with a performance code and the results compared with those taken in the IRT. The comparisons with the IRT shapes are performed to benchmark the performance code. The comparisons with the LEWICE shapes will show if the similar LEWICE shapes indeed show a similar loss in performance.

Ice Accretion Prediction Results

Part 1: Business Jet Airfoil

The first set of cases compares LEWICE with data taken on a Business Jet airfoil from an IRT test performed in July and August of 1995. This entry was the first of several IRT tests in the ‘modern airfoil’ study. This study is an effort by NASA Lewis to document ice shapes on airfoils which are of interest to industry. There are six cases which will be documented in this paper. Those six cases were chosen as they represent the longest exposure times to the icing environment. This criteria was used as it was expected that these cases would be the most difficult for LEWICE to predict the ice shape. All six cases were 45 minute runs at 175 knots and an angle of attack of 6°. The cases are presented in the order they were ran in the tunnel. The other tunnel conditions are given below.

Case 1: T_s=-5 °C, LWC=0.54 g/m^3, MVD=20 µm

Case 2: T_s=-6 °C, LWC=0.41 g/m^3, MVD=20 µm

Case 3: T_s=-10 °C, LWC=0.43g/m^3, MVD=20 µm

Case 4: T_s=-10 °C, LWC=0.6 g/m^3, MVD=15 µm

Case 5: T_s=-15 °C, LWC=0.41g/m^3, MVD=20 µm

Case 6: T_s=-15 °C, LWC=0.54g/m^3, MVD=20 µm

The results for case 1 are shown in Figure 1. This is a glaze ice shape with both an upper and lower horn. The LEWICE prediction is very good at capturing the overall shape of the experiment. The horn thickness is different however. This could be due to errors in the flow solver or in directing the runback water. If more runback were diverted to the lower surface, the prediction would improve.

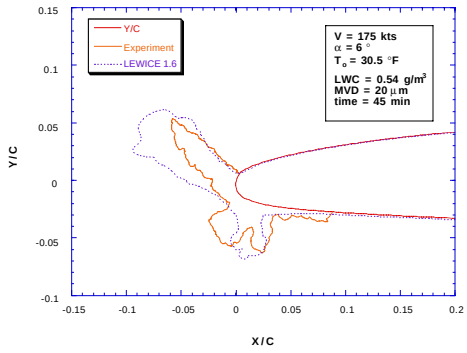

FIGURE 1. LEWICE Comparison for Case 1

Normally, this is the extent of comparison which has been done with LEWICE. A more quantitative comparison is given in Table 1. This table shows the measured values of horn length, horn width and horn angle for both the experimental ice shape and for LEWICE. These values were measured manually by selecting points off the ice shape plot. A tool on the spreadsheet package was used to retrieve coordinates from the plot. This is represented in Figure 2.

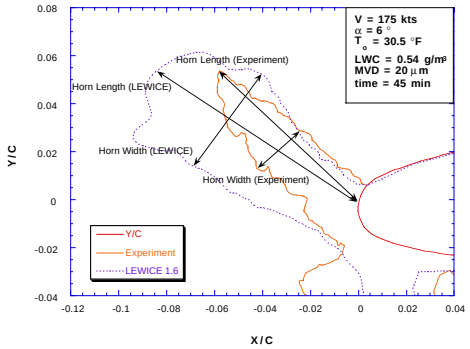

FIGURE 2. Measurement Location for Quantitative Results

TABLE 1. Horn Sizes for Case 1

Measurement	LEWICE	Exp.	Diff.
U. Horn Thick	91.4 mm	72.2 mm	19.2 mm
U. Horn Width	43.9 mm	21.4 mm	22.5 mm
U. Horn Angle	145.8°	140.7°	5.1°
L. Horn Thick	43.2 mm	45.7 mm	-2.5 mm
L. Horn Width	28.7 mm	45.2 mm	-16.5 mm
L. Horn Angle	227.9°	254.9°	-27°

The length was measured for both shapes from a common point on the airfoil so that the difference in horn angle was meaningful. Both the horn lengths and horn widths were measured at the maximum values for both shapes. Therefore horn width was measured at a different point for the LEWICE shape than for the experimental shape. However, horn width was always measured perpendicular to the length measurement. For shapes where the maximum horn length had a flat surface, the horn angle was measured from the center of the horn. The horn angle was measured from the airfoil surface, resulting in reported horn angles of $90° < \theta < 270°$.

This table shows that the overall shape appears to be qualitatively similar to the experiment primarily because of the good agreement to the upper horn angle. Despite the relatively large difference of 27° in the lower horn angle, the difference appears to be less due to the difference in lower horn width. The differences in horn size for this case show the trend of overprediction on the upper surface and underprediction on the lower surface. This could be due to an error in using the potential flow solution or in the modeling of the surface water runback. Another explanation is that LEWICE predicted transition too early in the boundary layer, since both horns form closer to the stagnation point in the LEWICE prediction.

Case 2 is shown in Figure 3. Contrary to the previous comparison, the LEWICE prediction looks very poor in comparison to the experimental ice shape. It is, along with Case 4, the worst comparison found so far with version 1.6 of LEWICE. The upper horn size is over twice as long as the IRT shape and the horn angle is not matched very well at all. LEWICE also predicts a single horn shape and does not predict the lower horn seen in the IRT shape.

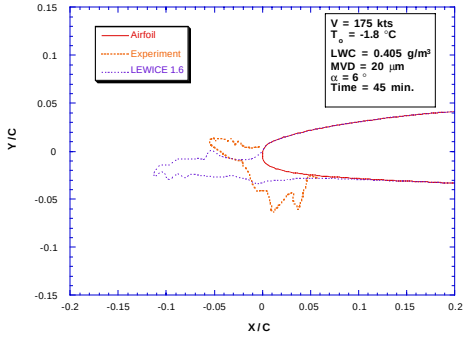

FIGURE 3. LEWICE Comparison for Case 2

TABLE 2. Horn Sizes for Case 2

Measurement	LEWICE	Exp.	Diff.
U. Horn Thick	105.2 mm	51.2 mm	54 mm
U. Horn Width	26.1 mm	18.7 mm	7.4 mm
U. Horn Angle	210.1°	162.8°	47.3°
L. Horn Thick	26.1 mm	41.4 mm	-15.3 mm
L. Horn Width	----------	31.9 mm	----------
L. Horn Angle	209.5°	260.1°	-50.6°

Table 2 shows the measured values for horn size and angle as performed for the Case 1. Even though the magnitudes are different, a similar trend is seen in the comparison. The upper horn is much larger in size while the angle is lower than the experiment. The lower horn is smaller and the lower horn angle is higher. Although a true horn is not seen in the LEWICE case, a horn angle was calculated from the thickest point on the lower surface. This makes the measurement susceptible to error, but this error will be much less than the difference in horn angle given.

In terms of area, the upper horn for Case 2 is nearly three times (2.86) the area of the IRT shape, but this difference is only 10% more than the area ratio for the Case 1 shapes (2.6 area ratio). This ratio does not compare the true horn areas, but simply the area calculated by taking horn length times horn width. This emphasizes that the qualitative comparison of ice shapes is driven by horn angle rather than size. This case also shows that since similar trends are seen in the data, the same physical mechanism can be used to explain the differences. The three theories to date are 1) poor flow solution from the potential flow code; 2) poor distribution of runback water; and 3) poor prediction of transition to turbulent flow. As will be shown later, the errors induced by the potential flow solver are indeed partially responsible for this result.

Case 3 shows the comparison for the next set of conditions in Figure 4. This is a colder condition and shows more of a mixed ice shape which is captured well by LEWICE. A single horn shape is produced with a horn angle which is again lower than the IRT shape. The quantitative comparison is shown in Table 3. Since there is only a single horn on both shapes, no lower horn data is presented in the table.

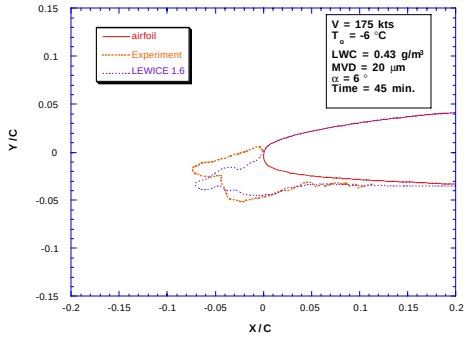

FIGURE 4. LEWICE Comparison for Case 3

TABLE 3. Horn Sizes for Case 3

Measurement	LEWICE	Exp.	Diff.
Horn Thick	69.5 mm	68.3 mm	1.2 mm
Horn Width	36 mm	45.3 mm	-9.3 mm
Horn Angle	202.1°	189.7°	12.4°

The quantitative comparison between LEWICE and the IRT shape is very good for this case. In particular, the horn length is very well predicted. The horn is narrower which also accounts for the difference in horn angle. The trends in the data are still similar to the previous two cases. The upper horn is slightly larger and the horn angle is lower for LEWICE when compared to the IRT shape.

Figure 5 shows the comparison for Case 4 of the first data set. The condition is at the same temperature, velocity and angle of attack as for Case 3, but at a higher LWC and smaller drop size. The difference between experiment and LEWICE is even more staggering when you consider the small difference in tunnel conditions for the Cases 3 and 4. Case 3 was predicted very well while the prediction in Case 4 is very poor. The experiment shows a mixed glaze ice shape similar to that shown in Figure 4 while LEWICE predicts a double horn glaze ice shape. Additionally, the upper horn on the LEWICE shape makes a sharp upward turn indicative of a numerical problem in the code.

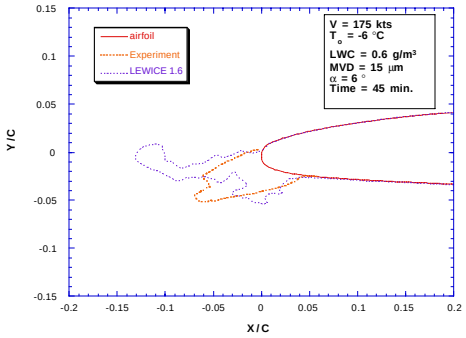

FIGURE 5. LEWICE Comparison for Case 4

TABLE 4. Horn Sizes for Case 4

Measurement	LEWICE	Exp.	Diff.
U. Horn Thick	123.6 mm	57.5 mm	66.1 mm
U. Horn Width	26.1 mm	20.7 mm	5.4 mm
U. Horn Angle1	189.8°	199.6°	-9.8°
U. Horn Angle2	143.2°	----------	----------
L. Horn Thick	39.7 mm	82.2 mm	-42.5 mm
L. Horn Width	29.6 mm	22.7 mm	6.9 mm
L. Horn Angle	258.6°	209.6°	49°

Table 4 shows the quantitative results for this case. Since LEWICE shows a double horn shape, results are presented in that manner. The values for the IRT shape were taken by dividing the shape down the center, as the bottom half of the ice shape is longer than the upper half. The upper horn for the LEWICE shape was divided into two sections at the point where the horn turns upward. The horn length reported is the distance from the surface to the turning point added to the distance from this point to the end, not the distance from the surface to the tip as measured for the other cases. The first horn angle for the upper surface represents the angle from the surface to the point where the shape turns upward and the second angle measures from this point to the tip.

This case shows the trends from the previous cases. The upper horn is overpredicted while the lower horn is underpredicted. The lower horn angle is much lower than shown in the experiment. This can be attributed to the three theories stated earlier. In addition, the prediction may be worse due the roughness prediction made by LEWICE. The roughness model was based on experimental roughness measurements made in the IRT at drop sizes of 20 microns. The smaller drop size could have a smaller roughness. Drop size changes do not have a large effect on the roughness prediction in LEWICE, but may have a larger effect in reality.

Cases 5 and 6 are rime ice shape comparisons to the IRT data and are shown in Figures 6 and 7. Quantitative results are listed in Tables 5 and 6. For a rime shape, the horn length is considered to be the maximum ice thickness. Both results show a similar shift in horn angle.

TABLE 5. Horn Sizes for Case 5

Measurement	LEWICE	Exp.	Diff.
U. Horn Thick	70 mm	49.4 mm	20.6 mm
U. Horn Width	30.2 mm	36 mm	-5.8 mm
U. Horn Angle	214.9°	199°	15.9°

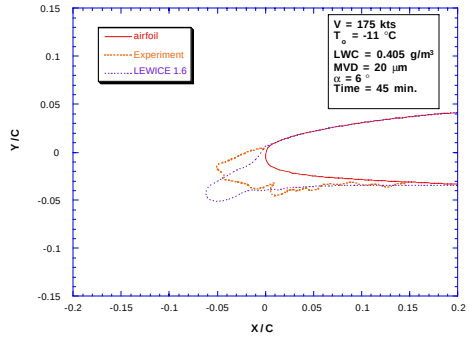

FIGURE 6. LEWICE Comparison for Case 5

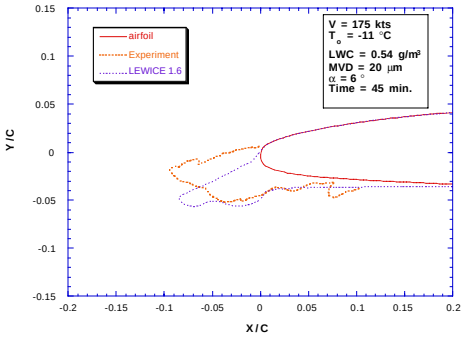

FIGURE 7. LEWICE Comparison for Case 6

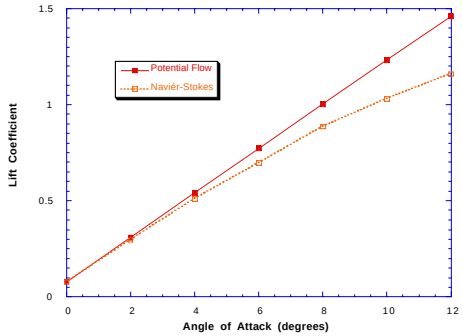

FIGURE 8. Predicted LiftComparison for Two Flow Codes

TABLE 6. Horn Sizes for Case 6

Measurement	LEWICE	Exp.	Diff.
U. Horn Thick	87.4 mm	87 mm	0.4 mm
U. Horn Width	36.4 mm	46.9 mm	-10.5 mm
U. Horn Angle	207.8°	189°	18.8°

These results support the theory that some of the errors in prediction are due to errors in the potential flow solution. The potential flow solution will usually overpredict lift, especially for higher angles of attack. This is shown in Figure 8 which plots lift versus angle of attack for the potential flow solver and for the Naviér-Stokes code. This shows that for a 6° angle of attack, the lift is overpredicted by 0.076. LEWICE predicts the same lift at 5.3° that is predicted by the Naviér-Stokes code at 6°.This factor can be accounted for in LEWICE by running the cases at the lower angle of attack instead of the actual angle of attack. Further investigation of this effect is planned for a future paper.

Part 2: Commercial Transport Airfoil

The second set of cases shows the LEWICE predictions compared to an IRT test performed on a commercial transport airfoil which is representative of a tailplane section. The results of this test are presented in another paper at this conference[8]. There were three conditions which were used in this comparison. These cases were selected as they were the longest runs in that test entry. The cases were at an angle of attack of 0° and a Mach number of 0.4. Other conditions are listed below.

Case 7: V = 250 kts, T_0 = 0 °C, LWC = 0.41 g/m^3, MVD = 20 µm, t = 22.5 min

Case 8: V = 248 kts, T_0 = -12 °C, LWC = 0.34 g/m^3, MVD = 15 µm, t = 29.3 min

Case 9: V = 250 kts, T_0 = -6.3 °C, LWC = 0.34g/m^3, MVD = 21 µm, t = 28.3 min

The comparisons for Case 7 are shown in Figure 9 and Table 7. Overall, the LEWICE prediction is very good, especially for a glaze horn formation. The general shape is captured except for a slight overprediction of the upper horn. The quantitative data in the table reflects this as well. The difference in horn angle measured is attributable to the technique used which measures from the airfoil to the tip of the horn. The upper horn of the LEWICE prediction starts drooping at the end. The difference in horn angle shows a slight angle of attack effect seen in the previ-

ous cases. It is not as pronounced here, since LEWICE more closely predicts the actual lift at lower angles of attack.

TABLE 7. Horn Sizes for Case 7

Measurement	LEWICE	Exp.	Diff.
U. Horn Thick	64.4 mm	46.9 mm	17.5 mm
U. Horn Width	21.3 mm	29.4 mm	-8.1 mm
U. Horn Angle	156°	135.6°	20.4°
L. Horn Thick	45.5 mm	42.9 mm	2.6 mm
L. Horn Width	33.9 mm	31.7 mm	2.2 mm
L. Horn Angle	230°	218.7°	11.3°

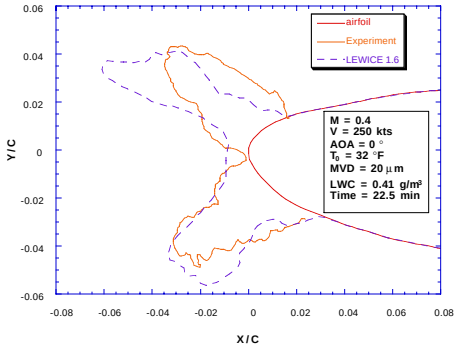

FIGURE 9. LEWICE Comparison for Case 7

Figure 10 shows the prediction for Case 8 which is a rime condition. The prediction is very good, as would be expected. This case also shows that there is not much of a lift effect in the ice shape prediction. Table 8 shows the quantitative comparisons for this case.

TABLE 8. Horn Sizes for Case 8

Measurement	LEWICE	Exp.	Diff.
Horn Thick	52.6 mm	45.6 mm	7 mm
Horn Width	28.1 mm	27.9 mm	0.2 mm
Horn Angle	180°	175.7°	4.3°

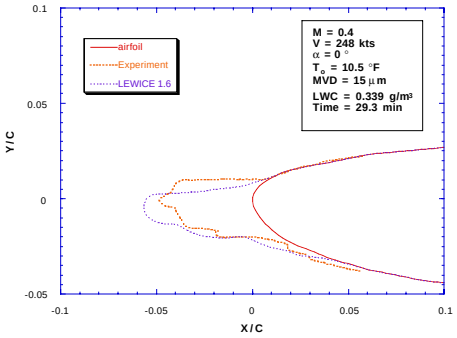

FIGURE 10. LEWICE Comparison for Case 8

Figure 11 shows the results for Case 9 which is more of a mixed icing condition. LEWICE did not predict this as well as the previous two cases. The predicted ice shape is longer and narrower than the IRT shape. Table 9 shows this result quantitatively. In general, LEWICE has the most difficulty predicting mixed condition ice shapes. This may be attributable to the ice growth mechanism applied in LEWICE which favors the prediction of classic glaze ice horns.

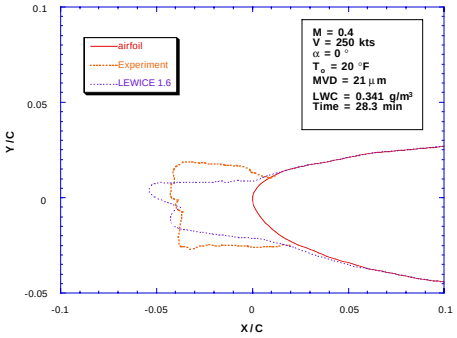

FIGURE 11. LEWICE Comparison for Case 9

TABLE 9. Horn Sizes for Case 9

Measurement	LEWICE	Exp.	Diff.
Horn Thick	49.7 mm	36.8 mm	12.9 mm
Horn Width	26.5 mm	41.6 mm	-15.1 mm
Horn Angle	183.2°	175.9°	7.3°

Iced Airfoil Aerodynamic Analysis

One of the difficulties associated with evaluation of ice shape prediction codes, is the lack of criteria for determination of the quality of the prediction compared to measured values. One measure of comparison has been outlined above and is based on a strictly geometrical evaluation. Another approach is to examine the aerodynamic impact of both experimental and computational ice shapes and to base an assessment of the similarity on aerodynamic parameters such as lift, drag or pressure distribution.

In order to take a look at what that might entail, we examined the flow fields associated with the experimental and computational ice shapes formed on the business jet airfoil section from Runs a and b, described in the previous section. The examination consisted of running the flow field module of the LEWICE/NS[9] code, using the shapes shown in Figures 1 and 3. The code results are then examined by evaluating the pressure distribution over the iced airfoil shape, the Mach number contours in the region near the iced airfoil, and the changes in lift compared to the clean airfoil.

The flow field module currently used in LEWICE/NS at LeRC is the ARC2D code developed by Steger[10] and Pulliam.[11] The grid code used in LEWICE/NS is a hyperbolic grid generator developed by Barth.[12] Other codes can be substituted for these, however these codes have worked well in the past for ice shape profiles and were thus retained for this examination.

Case 1

The first case examined was the two ice shapes shown in Figure 1. The two shapes shown in that figure are qualitatively similar in that they have the same ice growth limits along the surface, they both display a typical glaze-type horn growth, they have horns protruding in the same general direction, and these horns are approximately of the same length. There are however some obvious differences in the ice shapes, most notably the horn widths and the roughness level of the surface.

The first step in the process is the creation of grids for the two iced airfoil shapes. The grid generation process required some minor manipulation of the geometry, such as elimination of some of the deep convex cavities and smoothing of the surface to eliminate small irregularities. This was necessary in order to prevent highly skewed grid cells or crossing grid lines and is thus a limitation of the method. Unstructured grid codes are certainly available and could be applied to such a geometry however, this study concentrated on the more conventional structured grid approach and is thus interested in the limitations imposed by such methods.

The grids developed for the two ice shapes are shown in Figures 12 and 13. Comparing these figures to Figure 1 indicates the modifications that were necessary to create the grids. The modifications were much smaller than the differences between the two ice shapes and the resulting grid preserves the nature of both shapes. However, the differences do suggest that further studies may be necessary to determine the influence of such modifications on the resulting aerodynamics.

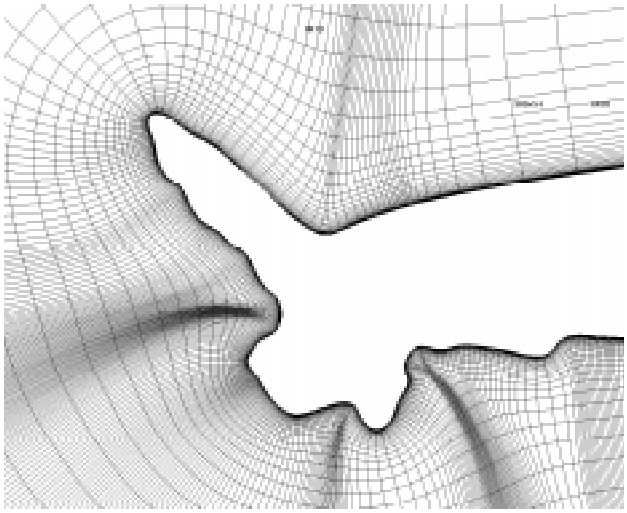

FIGURE 12. Grid for IRT ice shape on business jet wing section. Case 1.

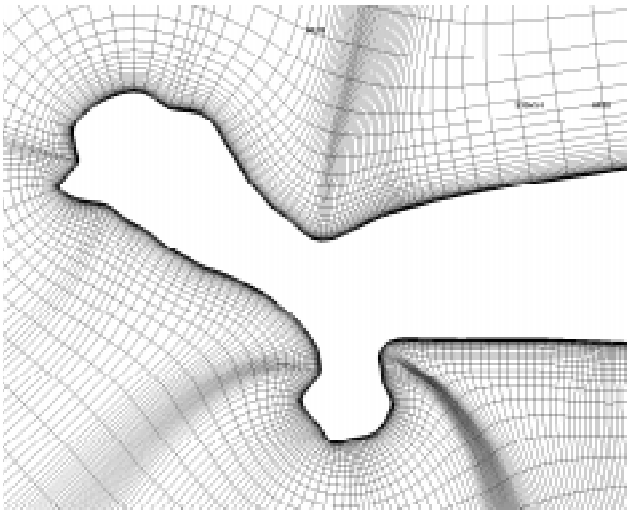

FIGURE 13. Grid for LEWICE ice shape on business jet wing section. Case 1.

Once the grids have been developed, the flow field calculations are obtained for several angles of attack at the flow conditions specified in Figure 1. The results of these calculations can be examined on several levels. For this discussion, the integrated lift values and mach number contour plots will be examined. The lift values are used to get a measure of the overall effect of the ice shapes on the airfoil performance and as a means of simply comparing the two ice shape profiles to each other and to the clean airfoil. The mach number contours are used to obtain a better understanding of the differences in the detailed fluid dynamics developed by these geometries.

Figure 14 shows a plot of the lift as a function of angle of attack for the two ice shape profiles as well as the clean airfoil geometry. The plot indicates that both ice shape profiles reduce the lift of the airfoil over most of the range of angle of attack values. Interestingly, the lift values calculated for the ice shapes at 12 degrees are larger than the results obtained for the clean airfoil. This suggests that the aerodynamic calculation at this incidence angle must not be capturing the vortex shedding process properly. This is an area for further computational investigation.

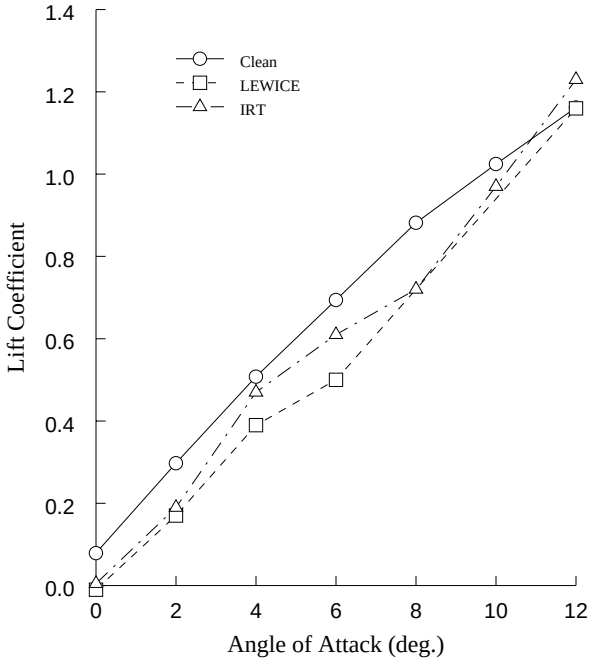

FIGURE 14. Lift-alpha plot for the clean airfoil, LEWICE ice shape, and IRT ice shape. Business jet wing section.

The other point of interest is that it is not clear from this evaluation whether the differences in ice shape are critical for determination of the resulting performance degradation. It does appear that the LEWICE generated shape has consistently lower lift values than those of the IRT produced shape. This suggests that, for this icing condition, the LEWICE result is conservative with respect to lift loss.

Looking at the mach number contours gives a better understanding of the differences that exist between the two shapes and may help in understanding the influence of various ice shape features. For this discussion, the six degree angle of attack condition will be examined. Figures 15-17 show the

contours for the clean, IRT produced, and LEWICE generated ice shapes, respectively.

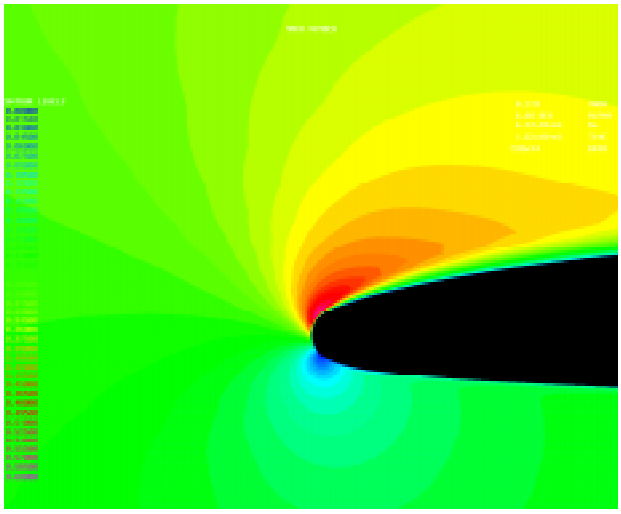

FIGURE 15. Mach number contours for business jet wing section. M_∞=0.27, Re=6.22x10^6, AOA=6°.

.

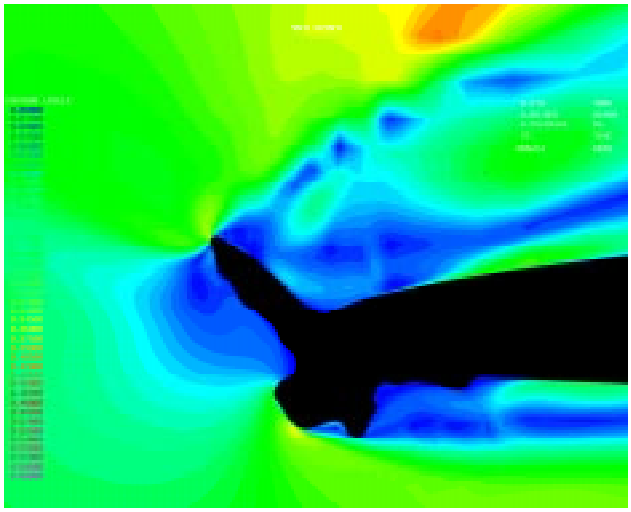

FIGURE 16. Mach number contours for IRT produced ice shape on business jet wing section. M_∞=0.27, Re=6.22x10^6, AOA=6°.

The contours for the clean airfoil show the acceleration around the suction peak on the upper surface as well as the low flow region near the stagnation point. The behavior in the regions aft of the leading edge is orderly and varies smoothly. There is no indication of recirculation regions or of possible separation. These contours are as expected for an airfoil of this type. The IRT ice shape produces a significant disturbance to the flow field even at this somewhat low incidence angle. Large vortical structures develop immediately behind both the upper and lower surface horns. Near the tip of the upper surface horn and trailing off behind it are another series of flow structures, most likely an indication of the shear layer developing between the main flow and the stagnant region near the airfoil surface. There are also large stagnant flow regions between the horns and aft of the lower surface horn.

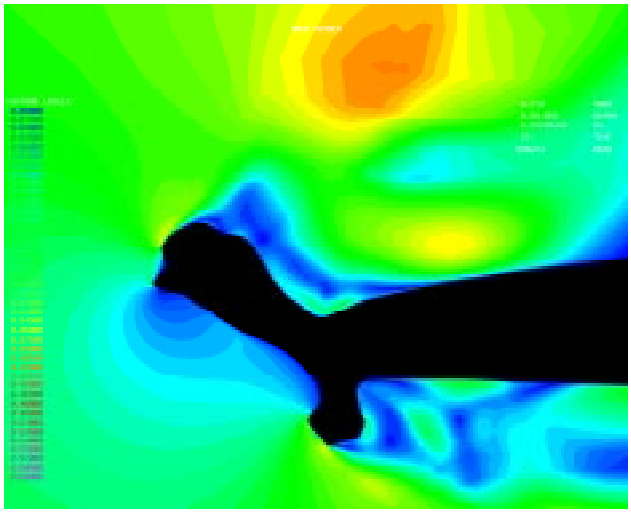

FIGURE 17. Mach number contours for LEWICE produced ice shape on business jet wing section. M_∞=0.27, Re=6.22x10^6, AOA=6°.

What is not evident here, but is shown in Figure 18, is the unsteady nature of this flow field. The vortical structures on the upper surface are swept back along the body and eventually shed into the main flow. This behavior results in a periodic fluctuation in the lift force produced by this iced airfoil geometry. The lift values shown in Figure 14 are thus actually time-averaged values of these fluctuations.

The contours for the LEWICE produced ice shape reveal similar flow structures to those of the IRT produced shape. It appears that, the flow fields of these two geometries are closer in nature to each other than either is to the clean airfoil flow. There are, however, notable differences between the two iced airfoil flows. The behavior aft of the upper surface flow displays the greatest qualitative difference between the two conditions. The LEWICE shape

appears to produce larger structures and a less distinct interface between the main flow and the region near the surface. This difference is best illustrated by comparing the lift versus time curves for the two runs shown in Figures 18 and 19.

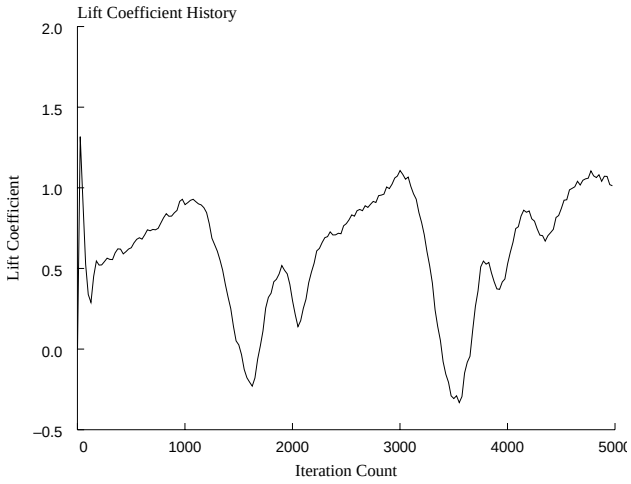

FIGURE 18. Lift history for IRT produced ice shape on business jet wing section. M_∞=0.27, Re=6.22x10^6, AOA=6°.

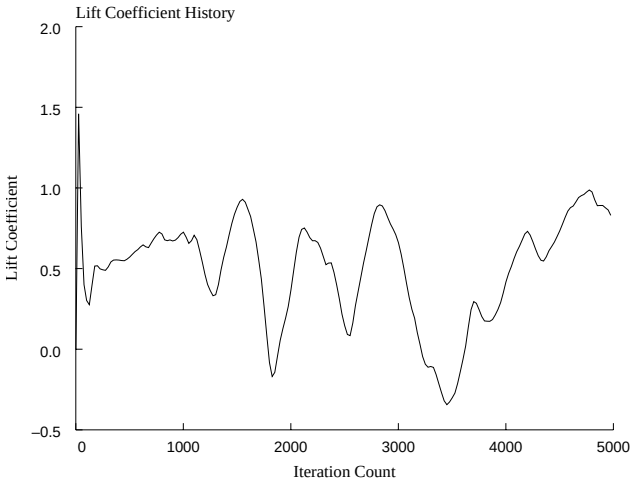

FIGURE 19. Lift history for LEWICE produced ice shape on business jet wing section. M_∞=0.27, Re=6.22x10^6, AOA=6°.

The lift history for the IRT produced ice shape shows a more distinct periodic behavior than does the lift history for the LEWICE produced ice shape. The differences in these curves, indicative of distinct vortex development patterns, produce the different time averaged lift values reported for these geometries, as shown in Figure 6. Basically, the size of the vortex structure created behind the horns and its shedding frequency determine the size and shape of the peaks in the lift history plot. The curve in Figure 18 has higher and broader peaks and smaller valleys than the curve in Figure 19, thus yielding the higher time-averaged lift value reported for the IRT produced ice shape.

Case 2

The second case examined was the ice shapes shown in Figure 3. In this case, the ice shapes are qualitatively different. The IRT produced shape has several distinct horns and a generally more blunt appearance than the LEWICE produced shape. As mentioned earlier, the quantitative measures of ice shape similarity are also worse for this case, especially the horn thickness and horn angle. Certainly, from a purely geometric point of view, it is clear that the LEWICE calculation did not result in an acceptable simulation of the ice shape produced in the IRT.

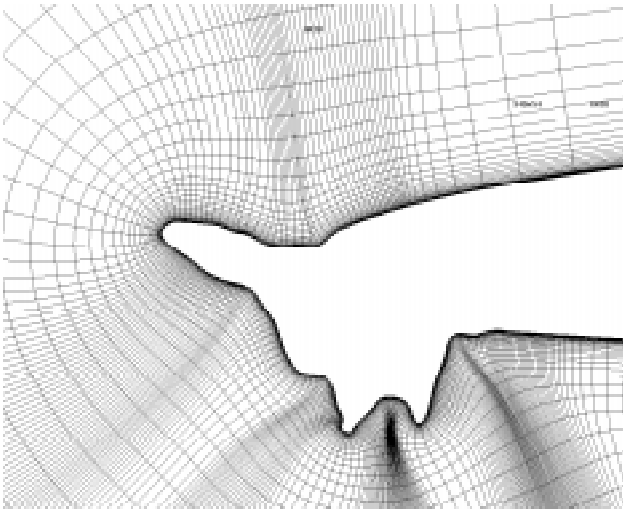

FIGURE 20. Grid for IRT ice shape on business jet wing section. Case 2.

The aerodynamic evaluation was accomplished in the same manner for this case as in the previous comparison. The grids used to model the ice shapes are shown in Figures 20 and 21.

FIGURE 21. Grid for LEWICE ice shape on business jet wing section. Case 2.

As was the case for the previous calculations, some modifications to the ice shape details was required to allow creation of the grids. This was limited to small concave structures along the surface and to the depth of the large concave region along the lower surface of the IRT shape. The grids were once again examined for skewness and to detect any intersecting grid lines.

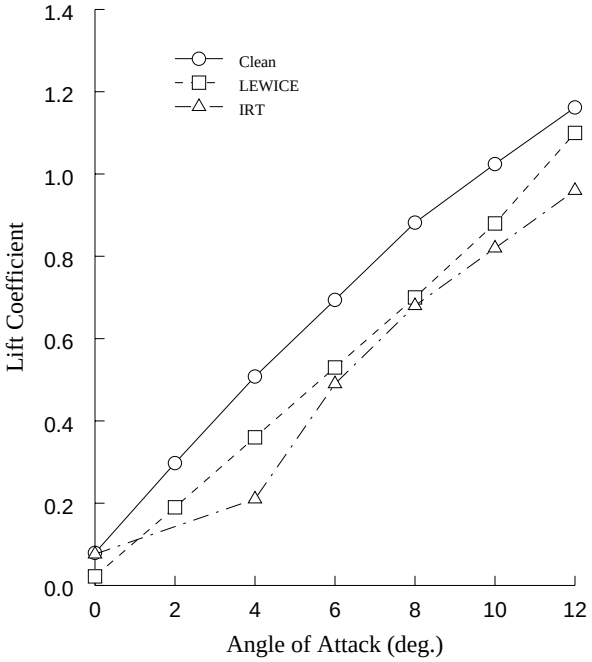

FIGURE 22. Lift-alpha plot for the clean airfoil, LEWICE ice shape, and IRT ice shape. Business jet wing section. Case 2.

The lift values for several angle of attack conditions are shown in Figure 23. As in the previous case, both ice shapes result in a loss of lift across the range of incidence angles. In this case, the differences in lift between the two shapes seem to be smaller than the difference between either case and the clean airfoil lift. This may be due to the lower overall lift values exhibited by this case when compared to the previous results.

The mach number contours, shown in Figures 23 and 24, reveal the details of the flow behavior. The 6 degree angle of attack case will be examined again. In this case, the lift values are much than for the previous case. The clean airfoil condition is the same as in the earlier discussion. Refer to Figure 15 when comparing to the mach number contours of the iced shapes.

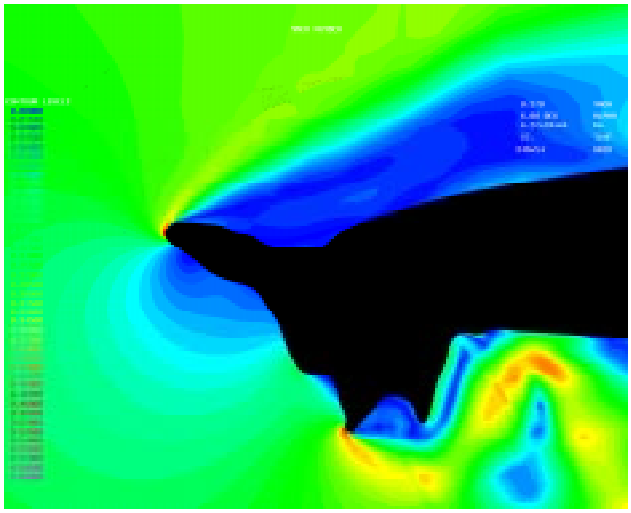

FIGURE 23. Mach number contours for IRT produced ice shape on business jet wing section. Case 2. M_∞=0.27, Re=6.22x10^6, AOA=6°.

The Mach contours indicate radically different flow behavior for the two case, as might be suspected from their geometric profiles. The IRT shape produces flow separation and vortex shedding on both the upper and lower surfaces. The LEWICE shape does not show any shedding behavior and flow separation regions are limited to the areas immediately surrounding the convex geometric structures. Since the lift values for these two cases compared quite well, this suggests that the lift value is not

necessarily a good indicator of adequate simulation. Further examination of the flow field for the LEWICE produced ice shape indicates how the lift values may have agreed for this condition.

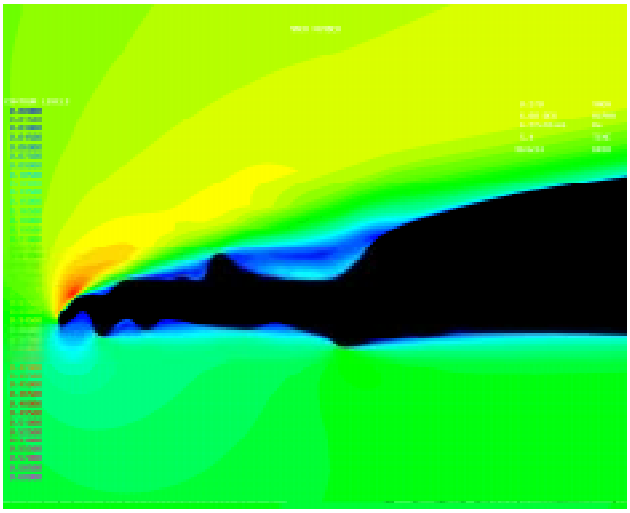

FIGURE 24. Mach number contours for LEWICE produced ice shape on business jet wing section. Case 2. M_∞=0.27, Re=6.22x10^6, AOA=6°.

Figure 25 reveals that this ice shape produced a trailing edge separation which was not present in any of the other cases at this angle of attack. This separation is most likely due the changes made to the boundary layer development by the ice shape at the leading edge. So, in this case the ice shapes and the flow field characteristics are quite different between the LEWICE shape and the IRT produced shape.

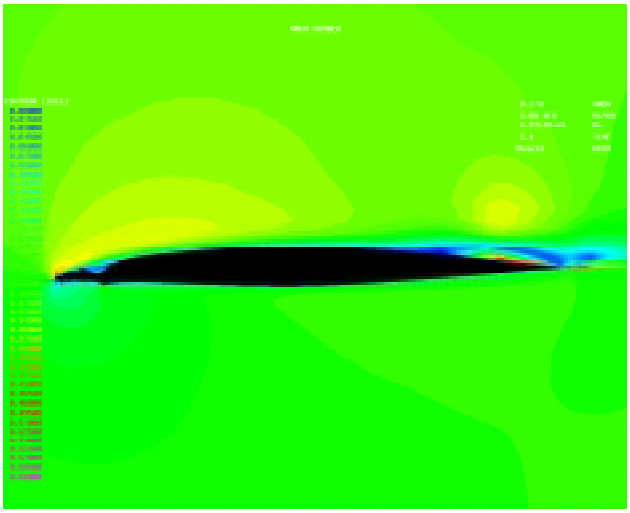

FIGURE 25. Mach number contours for LEWICE produced ice shape on business jet wing section. Case 2. M_∞=0.27, Re=6.22x10^6, AOA=6°.

Conclusions

A methodology has been proposed to validate the LEWICE and LEWICE/NS codes. This methodology includes quantitative comparison with experimental ice shape and comparison of aero performance degradation for the computed and experimental shapes.

The ice shape comparisons are mixed as some cases compare well to the data as others do not. Improvement is needed in the models for transition from laminar to turbulent flow in the boundary layer routine and in the overall prediction of heat transfer coefficient. The use of a potential flow solver also induces errors due to the higher lift which is predicted. Numerical errors are also evident in the longer cases. These errors will be addressed in the future. However, the differences between the predicted ice shape and the experimental data are not necessarily shown in the aero performance of the iced airfoil.

The behavior of the flow field associated with ice shape profiles can be examined to gain an understanding of the degree of agreement between simulated and measured ice shape profiles. One numerical value, such as the lift, should not be used without a more thorough investigation of all the parameters of interest. Some strategy must be developed that includes consideration of the geometry, the near and far field flow quantities, and of integrated force measurements. The strategy developed should be based on the needs of the analysis or design process being undertaken.

Perfect agreement of ice shape geometry between simulated and natural accretion would certainly be the best approach to guarantee that the simulated ice shape was an adequate substitute for the real thing. Lacking that perfect agreement, other tools, such as the CFD calculations used here or measured aerodynamic values, can be used to evaluate the adequacy of a ice shape simulation. A thorough and systematic examination of ice shape features (i.e. horn length, horn angle, horn width, number of horns, ice mass, ice extent along the surface, roughness level, etc.) and their effects on aero-

dynamic behavior must be undertaken in order to determine which of these features are important and how accurately they must be reproduced. Such a parametric study should be structured to produce information that will lead to the development of quantitative evaluation criteria.

Geometric comparisons alone are not adequate to determine the criteria for comparison. This study suggests that nominally similar ice shapes can produce significantly different aerodynamic effects. Details of the geometry can make large changes. This was seen in the first case where the shape of the upper horn played a role in the development of the separated flow region and ultimately in the lift generated for those geometries. Some consideration of aerodynamic impact should play a role in the evaluation of ice shape simulation.

References

1 Wright, W. B. and Bidwell, C. S., "Additional Improvements to the NASA Lewis Ice Accretion Code LEWICE," NASA TM (AIAA-95-0752), Jan. 1995.

2 Wright, W.B., "Users Manual for the Improved NASA Lewis Ice Accretion Code LEWICE 1.6," NASA CR 198355,June 1995.

3 Wright, W.B., Bidwell, C. S., Potapczuk, M. G. and Britton, R. K., "Proceedings of the LEWICE Workshop," June 1995.

4 Wright, W.B., "Capabilities of LEWICE 1.6 and Comparison with Experimental Data," presented at the SAE/AHS International Icing Symposium, Sept. 1995.

5 Wright, W.B., and Potapczuk, M. G., "Computational Simulation of Large Droplet Icing," presented at the FAA Phase III Meeting, May 1996.

6 Bragg, M.B., "An Experimental Study of a NACA 0012 Airfoil with a Simulated Glaze Ice Accretion," NASA CR 179571, Jan. 1987

7 Olsen, W., Shaw, R., and Newton, J., "Ice Shapes and the Resulting Drag Increase for a NACA 0012 Airfoil," NASA TM-83556, Jan. 1983.

8 Addy, G.E., Potapczuk, M. G., and Sheldon, D., "Modern Airfoil Ice Accretions," NASA TM (AIAA - 97-0174), Jan. 1997.

9 Potapczuk, M.G., Al-Khalil, K.M., and Velazquez, M.T., "Ice Accretion and Performance Degradation Calculations with LEWICE/NS", NASA TM-105972, Jan. 1993.

10 Steger, J.L., "Implicit Finite Difference of Flow About Arbitrary Geometries with Application to Airfoils," AIAA-77-665, 1977.

11 Pulliam, T.H., "Euler and Thin Layer Naviér-Stokes Codes: ARC2D, ARC3D," *Notes for Computational Fluid Dynamics User's Workshop*, UTSI E02-4005-023-84, March 1994.

12 Barth, T., Pulliam, T.H., and Buning, P.G., "Naviér-Stokes Computations for Exotic Airfoils," AIAA-85-0109, Jan. 1985